Analysis of ray trajectories of flexural waves propagating over generalized acoustic black hole indentations

Wei Huang[1], Hongli Ji[1,*], Jinhao Qiu[1], Li Cheng[2]

[1] State Key Laboratory of Mechanics and Control of Mechanical Structures
Nanjing University of Aeronautics & Astronautics, Nanjing, China
E-mail: jihongli@nuaa.edu.cn
[2] Department of Mechanical Engineering, The Hong Kong Polytechnic University
Hung Hom, Kowloon, Hong Kong
E-mail: li.cheng@polyu.edu.hk

Abstract

An Acoustic Black Hole (ABH) indentation embedded in thin-walled structures has been proved remarkably useful for broadband flexural wave focalization, in which the phase velocity of the flexural waves and the refractive index of the media undergo gradual changes from the outside towards the center of the indentation. A generalized two-dimensional ABH indentation can be defined by three geometric parameters: a power index, an extra thickness and a radius of a plateau at the indentation center. The dependence of the energy focalization on these parameters as well as the energy focalization process is of paramount importance for the understanding and design of effective ABH indentations. This work aims at investigating the energy focalization characteristics of flexural waves in such generalized ABH indentations. The calculation of the flexural ray trajectories is conducted to reveal and analyze the wave propagation features through numerical integration of the eikonal equation from the Geometric Acoustics Approximation (GAA). The theoretical results are verified by both experiment using wave visualization technique based on laser acoustic scanning method and finite element (FE) simulations. Finally, the influence of the geometric parameters on the flexural wave focalization characteristics in ABH indentations is discussed in detail.

Keywords: Flexural Wave; Acoustic Black Hole; Focalization; Ray Trajectories

1. Introduction

The propagation of flexural waves in thin-walled structures such as plates has been arousing persistent interest, among which an increasing number of studies have been recently reported on flexural wave focalization utilizing the effect of Acoustic Black Hole (ABH) by means of thickness variations in structures [1-3]. In an ideal one-dimensional or two-dimensional ABH structure (in which the local thickness along one given direction $h(x)$ and the distance x satisfy $h(x) = \varepsilon x^m$, $(m \geq 2)$, the local phase velocity of the flexural waves gradually reduces to zero when reaching the zero-thickness region ($x = 0$) of the power-law-profiled area [4, 5], which warrants efficient wave focalization. Meanwhile, the gradually diminishing thickness in the plate

also results in a continuous variation of the refractive index of the waves. Owing to its lightweight and broadband wave trapping feature, ABH structures offer great potentials for a wide range of engineering applications through structure-borne wave control and manipulations.

However, imperfections are inevitable in any realistically achievable ABH structures due to the limited machining and manufacturing capability. Therefore, typical two-dimensional ABH structures studied in the literature usually contain a hole or a circular plateau of constant thickness at the center of the indentation [6-10]. It was shown that, despite the imperfect thickness profile, appreciable vibration damping can still be achieved by using a small amount of damping material in the thin-thickness region [7, 11]. One could surmise that energy focusing feature of the flexural waves still exists in imperfect ABHs due to the continuous variation of the refractive index within the indentation area and the focalized energy can be effectively dissipated in the area with high energy concentration. This would potentially increase the applicability of the ABH structures without the need for extra high-precision manufacturing.

On the other hand, generalized ABHs with modified profiles also help improve the venerable structural integrity existing in the ideal ABH structures. Achieving and enhancing the desired energy focalization capability of the ABH structures without compromising their structural integrity would reply on a good understanding of the energy transport process within the indentation, which eventually allows wave manipulation or system optimization. As a typical effort, five different lenses with different gradient refractive index distributions in thin plates were investigated in a previous work [12]. The gradient refractive index distributions, which were once defined in optical lens for light focusing, were realized by adjusting the local thickness of the thin plates. Numerical calculated displacement fields show that the focusing behavior of these lenses for flexural waves is similar to that in the optical lens for electromagnetic waves. Several new types of generalized ABH indentations were proposed and their energy focalization characteristics were investigated both numerically and experimentally and compared with those of ideal ABHs [13]. The results show that, despite the obvious energy focalization in those generalized ABHs (even with a power index less than 2), the distribution of the focalized energy was quite different from that in an ideal ABH structure. The location of the energy concentration is found to deviate from the central area of the imperfect ABH indentation, downstream of the wave incidence. The above analysis, however, mainly focused on the final energy focalization phenomenon based on energy distribution maps, rather on the energy transport process. Nevertheless, these results confirm that the generalized ABHs can produce vibration damping effect similar to that in the ideal ABHs. For future application of the generalized ABHs in real structures, a thorough understanding on the

energy focalization process as well as the influence of various geometrical parameters is of paramount importance, which can only be made possible by systematically investigating the flexural ray trajectories in the indentation area.

Among possible theories for the calculation of the ray trajectory, the geometric acoustics method is most widely used. Several researches based on geometric acoustics have been reported on the derivation of governing equation and numerical calculation of flexural wave trajectories in plates with smoothly varying thickness. Krylov used Hamiltonian form of the geometrical acoustics to derive the ray path equation of wave propagation over a smooth axisymmetric indentation [14]. The validity conditions of the geometrical acoustics approximation (GAA) of flexural waves were also derived from the equation of motion of thin plates [15]. According to the GAA, the incoming flexural rays entering an ideal ABH indentation under certain incidence conditions would deflect towards and then focus to the center of the indentation [5, 10]. Existence of a stationary orbit for flexural waves and the centripetal characteristic of the rays inside the stationary orbit in the ideal ABH indentation with $m = 2$ were also exhibited [16, 17], in good agreement with the typical energy focalization phenomenon in ideal ABHs. The above work focused on ideal thickness profile, investigations on flexural ray trajectory in generalized ABH indentations with tolerable imperfections is lacking.

In this study, flexural ray trajectories are investigated to analyze the process of wave propagation and energy focalization through numerical integration of the eikonal equation from geometric acoustics approximation. The proposed method can also be used as a tool in the design of ABHs for wave focalization and manipulation in practical applications. The paper is organized as follows. In section 2, the theoretical background of the GAA and the proposed numerical integration scheme of the eikonal equation are introduced. The results obtained by direct numerical integration are then verified by both experiments based on a laser ultrasonic scanning technique and the power flow vectors (PFV) combined with finite element (FE) simulations in section 3. In section 4, the ray trajectories in both an ideal and two generalized two-dimensional ABHs with different geometrical parameters are investigated in detail to clarify the energy focalization characteristics in these generalized ABH indentations. Conclusions are drawn in section 5.

2. Generalized ABH Indentation and Theoretical Background

2.1. Description of the Generalized ABH Indentation

The generic form of a generalized ABH indentation is schematically shown in Fig. 1, whose thickness profile is described in the following general form:

$$h(r)= \begin{cases} h_1, & (r<r_1) \\ a(r-r_1)^m+h_1, & (r_1 \leq r \leq r_2) \\ h_2, & (r>r_2) \end{cases} \tag{1}$$
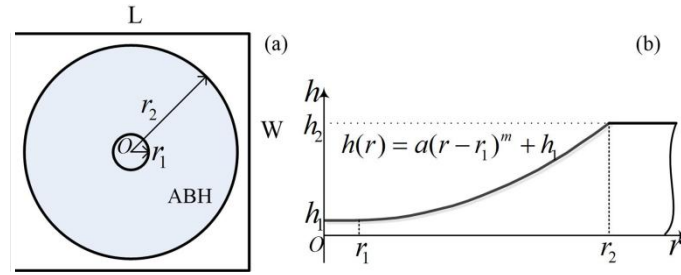

Fig. 1. Plate with a generalized two-dimensional acoustic black hole indentation.

For a plate with a given thickness and a fixed outer diameter of ABH, the generalized ABH indentation is characterized by three parameters (a power index m, an extra thickness h_1 and a radius of a plateau r_1 at the indentation center). In a practical ABH structure, the plateau usually serves a number of purposes. Firstly, it can improve the structural static properties and guarantee the structural integrity. Secondly, a plateau facilitates the mounting of other components such as viscoelastic material for damping and piezoelectric material for energy harvesting. Thirdly, it extends the ABH area so as to reduce the effective frequency region of the ABH [18]. In this work, generalized ABH indentations are divided into two categories. One is the conventional ABH indentations with a power-law profile with $h_1=r_1=0$. The other one is generalized ABH indentations with $h_1 \times r_1 \neq 0$. The former one leads to the ideal ABH structure when $m \geq 2$.

2.2. Eikonal Equation from Geometric Acoustics Approximation

The two-dimensional equation of motion governing the flexural waves in a thin plate with a variable local thickness $h(x, y)$ can be expressed as [19]

$$\nabla^2(D\nabla^2 w)-(1-v)\left(\frac{\partial^2 D}{\partial y^2}\frac{\partial^2 w}{\partial x^2}-2\frac{\partial^2 D}{\partial x\partial y}\frac{\partial^2 w}{\partial x\partial y}+\frac{\partial^2 D}{\partial x^2}\frac{\partial^2 w}{\partial y^2}\right)+\omega^2\rho h w=0 \tag{2}$$

where w is the transverse displacement of the plate; $D=Eh^3/12(1-v^2)$ the flexural rigidity; E the Young's

modulus; v the Poisson's ratio; ρ the density and ω the circular frequency. The solution of Eq. (2) in the conventional GAA writes

$$w = A(x, y)\exp(ik_p\varphi(x, y)) \tag{3}$$

where $A(x, y)$ is the amplitude; $\varphi(x, y)$ the eikonal of the quasi-plane wave; $k_p = \omega / c_p$ the wave number of quasi-longitudinal waves and c_p the wave phase velocity in the uniform plate. Substituting Eq. (3) into Eq. (2), both the real and imaginary parts of the resulting expression have to be equal to zero. By omitting the terms with second and higher derivatives of $A(x, y)$ and $\varphi(x, y)$, the so-called 'eikonal equation' for flexural waves in GAA yields [4]

$$|\nabla\varphi(x,y)|_4 = k_4\varphi(x,y)/k_{p4} = n_4(x,y) \tag{4}$$

where ∇ is the gradient operator. The validity conditions of the GAA is $|dk/dr| \ll k^2$. The $k(x,y) = 12^{1/4}k_p^{1/4}/(h(x,y))^{1/2}$ the wave number in the plate with variable thickness and $n(x,y)$ the location-dependent refractive index which can be expressed as a function of the plate thickness as [12]

$$n(x, y) = (h_2/h(x, y))_{1/2} \tag{5}$$

It can be seen from Eq. (5) that, despite of the intrinsically dispersive nature of the medium, the refractive index does not depend on the frequency of the wave, but is related to the geometric parameters of the plate. The broadband nature of the ABH structures has been proved [7, 20], which is limited by the characteristic size of ABH indentation. The analysis is valid above the characteristic frequency f_c, expressed as $\lambda = c_0/f_c \leq D_{ABH}$ [18, 21], where D_{ABH} is the diameter of ABH indentation and $c_0 = [\frac{\omega_2 E h_{22}}{12\rho(1-v_2)}]_{1/4}$ is the wave speed in the uniform portion of the plate. Above this frequency, the incoming wavelength starts to be equal to or less than the geometrical characteristic dimension of the ABH indentation.

Assuming $\mathbf{r}(s)$ is the position vector at a given point on the ray trajectory, and ds is a differential segment on the trajectory from the given point, as shown in Fig. 2. The directional vector of the ray trajectory is $\mathbf{s} = d\mathbf{r}/ds$. Since $\mathbf{s}$ is perpendicular to the equiphase surface, it should be parallel to $\nabla\varphi$. Therefore, $\mathbf{s} = \nabla\varphi/|\nabla\varphi|$, and eikonal equation from Eq. (4) is written as

$$\nabla\varphi(x,y) = n(x,y)\, d\mathbf{r}/ds \tag{6}$$

Performing derivative to arc length of trajectory s on both sides of Eq. (6) leads to the ray trajectory equation in gradient index medium as

$$\frac{d}{ds}(n(x,y)\frac{d\mathbf{r}}{ds}) = \nabla n(x,y) \tag{7}$$

The above ray trajectory equation for flexural wave in analogous to the optical ray equation determined by the Fermat principle. Translating the solution found for electromagnetic waves into the acoustic waves has been performed [22], and the flexural wave behaves like optical ray, which demonstrates the validity of the analysis. The ray trajectories depend on the local refractive index over the plate and initial incident condition based on GAA. The refractive index does not depend on the frequency of the wave, but is related to the geometric parameters of the plate. Therefore, the ray trajectories are not depending on the frequency. Since it is difficult to obtain the analytical solution of Eq. (7) in most cases, numerical calculations are introduced in the following section.
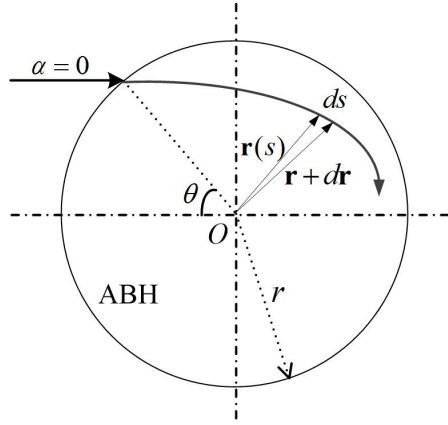
Fig. 2. Sketch of incident wave and wave trajectory.

2.3. Ray Trajectories Calculation by Taylor Expansion

To solve the ray trajectory equation, a numerical scheme is developed through Taylor expansion. Retaining the first and second order derivative terms, the position vector $\mathbf{r}$ in an adjacent region to the initial position vector $\mathbf{r}_0$ is expressed as

$$\mathbf{r} = \mathbf{r}_0 + \frac{d\mathbf{r}(s_0)}{ds}\triangle s + \frac{1}{2!}\frac{d^2\mathbf{r}(s_0)}{ds^2}(\triangle s)^2 \tag{8}$$

where $d\mathbf{r}(s_0)/ds = d\mathbf{r}/ds\,\hat{u}_{s=s_0}$ is the directional vector at the initial position of an incident ray and $\triangle s$ the step size. The truncation of the series warrants an error in the order of $(\triangle s)^3$. Likewise, $d\mathbf{r}/ds$ can be decomposed as

$$\frac{d\mathbf{r}}{ds} = \frac{d\mathbf{r}(s_0)}{ds} + \frac{d^2\mathbf{r}(s_0)}{ds^2}\triangle s \tag{9}$$

where $d^2\mathbf{r}/ds^2$ represents the curvature vector. Assuming $\mathbf{k} = d^2\mathbf{r}/ds^2$, one has

$$\begin{cases} \mathbf{r} = \mathbf{r}_0 + \mathbf{s}\triangle s + \dfrac{1}{2}\mathbf{k}(\triangle s)_2 \\ \qquad \mathbf{s} = \mathbf{s}_0 + \mathbf{k}\triangle s \\ \mathbf{k} = \dfrac{1}{n}[\nabla n - \dfrac{d\mathbf{r}}{ds}(\dfrac{d\mathbf{r}}{ds}\cdot\nabla n)] \end{cases} \qquad (10)$$

According to Eq. (10), the $\mathbf{k}$ is determined by initial incident conditions $\mathbf{r}(s_0)$, $\mathbf{s}(s_0)$ and local distribution of refractive index n in the ABH indentations. Then, $\mathbf{r}$ and $\mathbf{s}$ are obtained by choosing a $\triangle s$, which can be considered as new incident conditions. Ray trajectories are numerically achieved by repeating the above operation.

3. Experimental and Numerical Verifications

3.1. Experimental Setup and Test Sample

To validate the calculated ray trajectories, the wave propagation process in an ABH indentation in time domain was determined through experiments using wave visualization technique based on the laser acoustic scanning method [23-25]. Calculation results of the ray trajectories are compared with the observed wave fields. Figure 3 shows the experimental system used, which includes a laser generator (YAG laser, Ultra-100, Quantel corp., USA) for wave generation, an acoustic emission (AE) sensor (M31, Fuji Ceramics corp., Japan) for wave measurement, a pre-amplifier (A1002, Fuji Ceramics corp., Japan), an AE analyzer (AE9922, NF corp., Japan), a high-speed digitizer (PXI-5105, NI corp., USA) signal acquisition and an analog output module (cRIO-9263, NI corp., USA) for controlling a two-dimensional laser mirror scanner (TSH8203H, Century Sunny corp., China). The laser pulse scans the sample with a repeating frequency of 20 Hz.
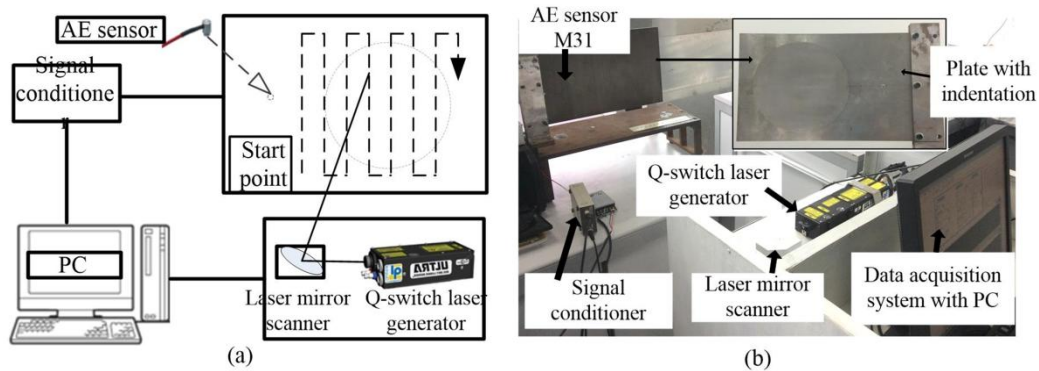

Fig. 3. Schematic diagram (a) and experiment setup (b) of the laser ultrasonic system.

The steel plate used in the experiment is shown in Fig. 4, which has a dimension of 350×240×5mm, clamped along one edge and free along all others. The indentation in the plate firstly went through a milling process with a positive allowance of 0.3-0.4mm. After tempering and aging treatment, machining operation finishes by wire-electrode cutting. The thickness profile of the indentation area in the steel plate used in the experiment follows $h(r)=7.34\times10^{-4}\times(r-20)^2+0.6, (20\leq r\leq100)$ (in mm). The characteristic frequency of the ABH indentation used in this work is 1398Hz. The AE sensor was fixed and located 150mm away from the central point on the symmetry axis, and the flat side of the plate was scanned over an inspection region (250×220mm) by rotating the two-dimensional mirror. The spatial scanning interval is 1 mm giving a total of 55,471 scanning points.
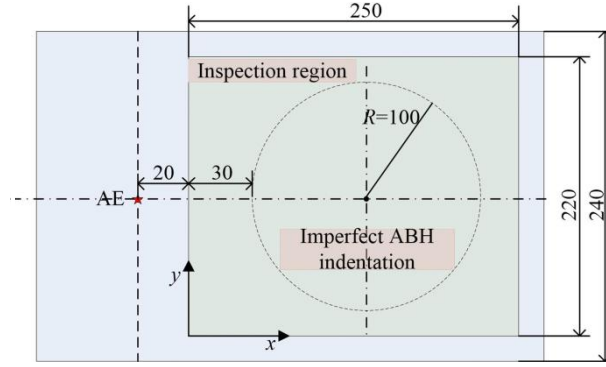
Fig. 4. Diagrammatic sketch of experimental plate.

3.2. Comparisons between the Measured Wave Fields and Calculated Ray Trajectories

The response of the AE sensor to the laser excitation at different scanning points was sampled and recorded. Based on the reciprocal theorem in elastodynamics, the obtained signals from the AE sensor can be used to reconstruct the dynamic acoustic wave field in the inspection region. One AE sensor was used to reconstruct the dynamic acoustic wave field under single point excitation. FE simulation on the same clamped-free steel plate with ABH indentation was also performed using the commercial FEM software Abaqus, with a tone burst force applied on the corresponding position of the AE sensor with a center frequency $f_{cent}=20$ kHz. The steel plate with $E=210\text{GPa}$, $\rho=7800\text{kg/m}^3$ and $v=0.3$ was meshed by using C3D8 elements under plane stress condition. A minimum of ten elements per local wavelength were used to guarantee the calculation accuracy in the FE model. The bandwidth of the frequency spectrum of the burst is from 16 kHz to 24 kHz. Our experimental results are obtained using a pass band filter (15 kHz-25 kHz), which is similar to the bandwidth of frequency spectrum of the burst tone used as the excitation. Since the

focalization position of waves is independent of the frequency, because the refractive index does not depend on the frequency, the wave focalization phenomenon is similar even though the bandwidth is slightly different.

Wave propagation process as well as the focalization characteristics in the ABH indentation is revealed in Fig. 5. The ray trajectories of flexural wave under a point excitation are calculated by the proposed method using numerical integration. Kirchhoff plate theory is used in the ray model, which has its own limitation in describing the bending motion in the high frequency range. The vibration pattern of a plate in the high frequency range undergoing anti-symmetrical Lamb-wave motion will retreat to the flexural mode when the wavelength becomes much greater than the thickness (Ra=λ/h>>1) [26]. In the steel plate with h=0.005m, the wavelength of the first-order anti-symmetrical Lamb-wave mode is equal to the thickness (Ra=λ/h=1) when the frequency is 0.593MHz. When the frequency is much lower than 0.593MHz, the plate theory will give enough accuracy. Although the Kirchhoff plate theory has lower accuracy than the Mindlin plate theory [27], their difference is only 1% at 25 kHz, which is highest frequency considered in this plate. As mentioned in section 2.2, the validity conditions of the GAA is ｜dk/dr｜<<k^2. The analysis of the ray trajectories based on GAA is valid when the frequency is far greater than 45.8Hz. Therefore, the analysis in our work is valid because the frequency range we analyzed belongs to all the above frequency ranges. The curves with arrows represent the ray trajectories. The step size of ray trajectory calculation is △s=0.0005m which ensures the convergence of the numerical calculation.

The wave fields are compared with the predicted trajectories. The comparison between the simulated displacement fields and the ray trajectories is shown in Fig. 5(a)-(c), while that between the measured wave fields and the calculated ray trajectories is shown in Fig. 5(d)-(f), demonstrating a good agreement between them. Results show that the circular wave-fronts are deformed when waves impinge into the ABH indentation. The ray trajectories are strongly curved and deflected from their original direction. Both the wave fields and the ray trajectories indicate that the flexural waves focus to a confined region slightly downstream of the central plateau. Part of the waves passes through the central plateau while others detour around it. The wavelength of the flexural wave is compressed as the thickness of the plate becomes thinner. In addition, the times of the wave fields are given in Fig. 5. It should be noted that the time t' is the time after compensation, which is a procedure to compensate for the pre-sampling time after the measurement is triggered. The time intervals between the corresponding wave fields are quite similar, which also shows a good consistency between the simulation and experiments. We believe that the comparison results can validate the prediction of flexural wave focalization phenomenon on one hand, and verified the results of the numerical calculation of

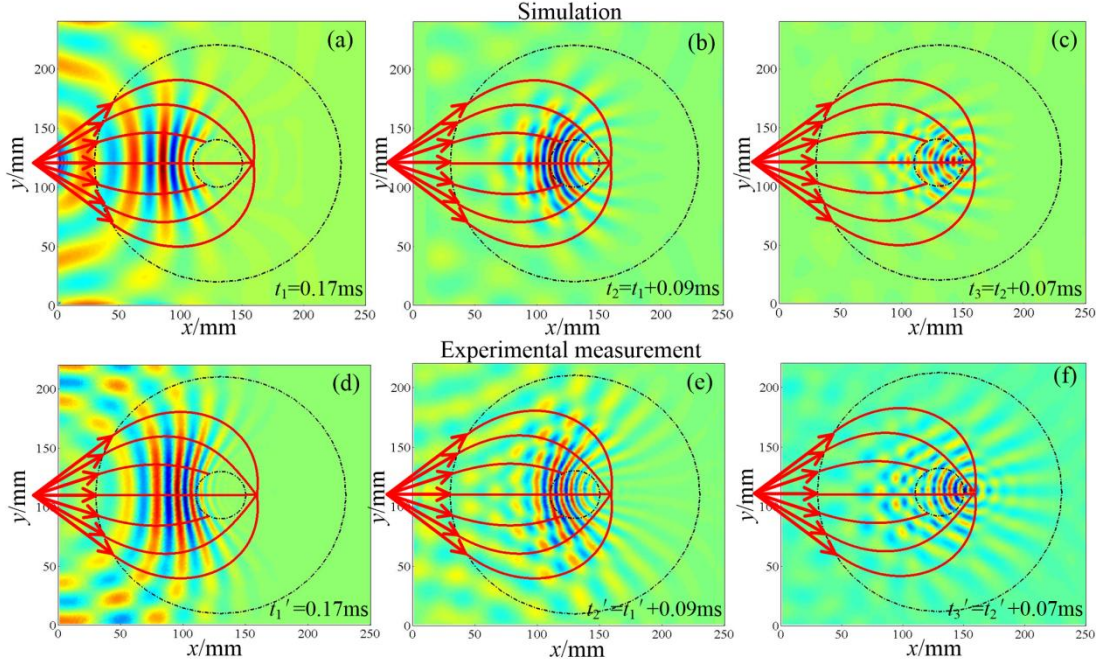ray trajectories from the GAA on the other hand.

Fig. 5. Comparison between the simulated wave fields with the ray paths ((a)-(c)) and the measured ones ((d)-(f)). The curves with arrows represent the ray trajectories (m=2, r_1=0.02m, h_1=0.0006m).

3.3. Comparisons between the Power Flow Vectors and Ray Trajectories

The ray trajectories calculated by the GAA are also compared with the power flow vector (PFV) which is defined as the rate of energy passing through a cross section of a unit area in a structure as a supplementary indicator to describe the energy transport path. The time averaged net power flow is defined as

$$P(t) = \lim_{T \to \infty} \frac{1}{T} \int_0^T F(t) \ v(t) \ dt \tag{11}$$

where $F(t)$ and $v(t)$ are the instantaneous force and the corresponding velocity at a point, t and T are the time and observation period. By using the 'two-transducer' method [28-30], the active power (also called time-averaged power or intensity) is obtained as

$$I_x = \frac{2\sqrt{Dm'}}{d'} \text{Im}\{G_{12}\} \tag{12}$$

where I_x is the active power in the x- direction from one point to adjacent point; G_{12} the cross-spectrum of velocity signals; d' the spacing; m' the mass per unit area of the plate. Im represents the imaginary part. Eq. (12) is applicable in both x- and y- directions of the plate ($\mathbf{I} = (I_x, I_y)$). The PFV gives both the magnitude and the direction of the energy flux.

In order to make the comparison of the local deflection of wave propagation direction between ray

trajectories and PFV, a deflection angle of ray trajectory is defined as the angle between the local directional vector and x- direction as

$$\beta = \arcsin(I_y /|\mathbf{I}|) \tag{13}$$

Flexural wave propagation in the ABH indentations with $h_1 \neq 0$, $r_1 = 0$ is analyzed in this section as an example, and the propagation directions of the flexural waves are analyzed and compared using the deflection angle. As shown in Fig. 2, θ is the azimuth angle of the incident wave. In the present analysis, a plane wave ($\alpha = 0$, α is the angle between initial wave vector and x- directions) is considered in the simulation. In all following cases, the size of the plate is 0.24×0.24×0.005m, and the radius of the ABH indentation is $r_2 = 0.1$m.

The PFV, the displacement fields as well as the typical ray trajectories are plotted in Fig. 6, with a zoomed-in figure given by Fig. 6(b). It can be seen that the distribution of the PFV agrees well with the ray trajectories calculated by GAA in all ABH indentation cases. To some extent, energy focalization can still be obtained in this ABH indentation, slightly downstream of the central point. However, the waves do not converge to a single point. Figure 7 compares the deflection angles on four typical rays used in Fig. 6, calculated from the ray trajectories and from PFV, respectively. It shows a fair agreement for the deflection of propagation direction (with an error less than 5 degree as compared with PFV), which indicates that the analysis of ray trajectories is valid for predicting and investigating the characteristics of flexural wave propagation in the plate with generalized ABH indentation.
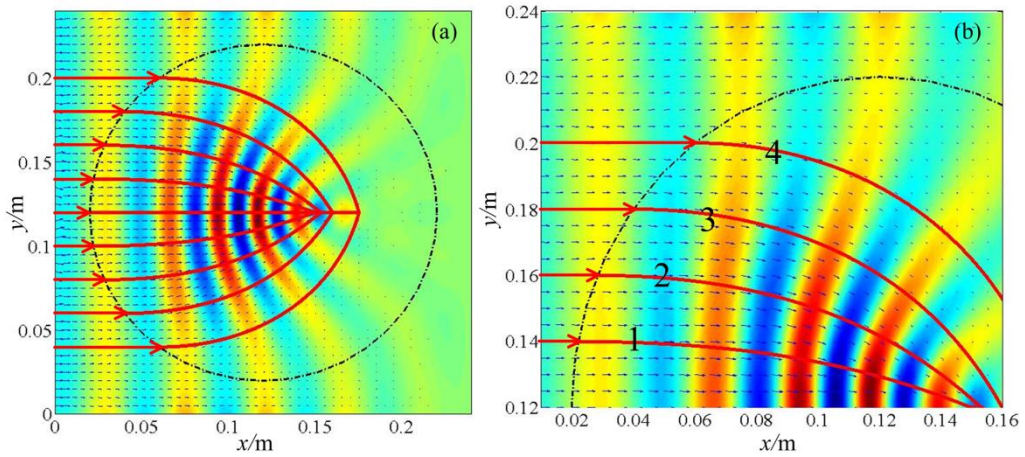

Fig. 6. Comparison of power flow vectors (FEM) with the ray paths (GA) in the ABH indentation with $m = 2$, $h_1 = 0.001$m.
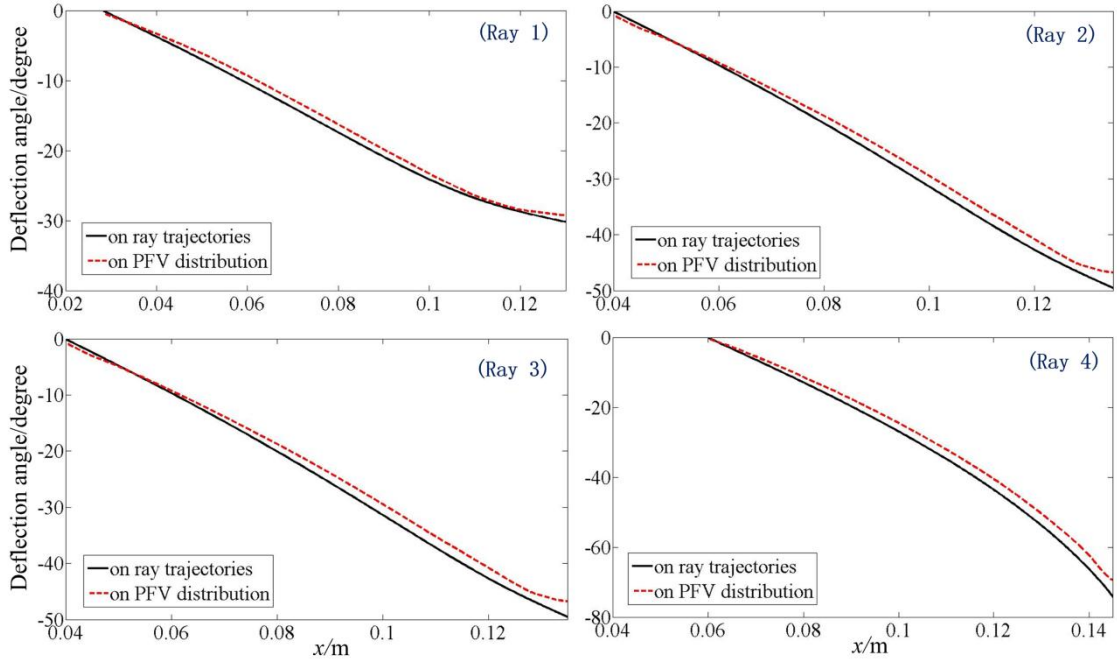
Fig. 7. Comparison of deflection angle on four ray trajectories with the deflection angle of power flow vectors on the corresponding position.

4. Flexural ray Trajectory in Different Types of ABH

Numerical analyses on the ray trajectories in three types of ABH indentations are conducted in the following sections: one is the conventional ABH indentation with power-law profile ($h_1 = r_1 = 0$) and the other two contain generalized ABH indentations with $h_1 \neq 0, r_1 = 0$ and $h_1 \neq 0, r_1 \neq 0$. The effect of geometric parameters in the generalized ABH indentations is investigated.

4.1. Flexural Ray Trajectory in Conventional ABH Indentations with a Power-law Profile

Numerical analyses are performed to illustrate the flexural ray trajectories in conventional ABH indentations with a power-law profile ($h(r) = \varepsilon r^m$) in the first place. Figure 8 reveals the effect of the power index m on the ray trajectories with a plane wave incidence. It can be seen that the parallel trajectories outside the indentation are curved towards the ABH indentation. The curvature of the flexural rays rotating to the center becomes greater when the index m increases, resulting in better focalization to the central point. More waves will escape from the ABH area with $m = 1.5$ as compared with the case of the ideal ABH indentation with $m = 2$ and $m = 3$. With $m = 2$, majority of the flexural waves penetrate into the central point as shown in Fig. 8(b). There exists a critical trajectory separating the rays that converge to the center and those that diverge in the ideal ABH indentation. The existence of critical trajectory is consistent with the reported

stationary trajectory in ideal ABH structure with $m=2$ [17]. In the present case, the critical trajectory corresponds to $\theta=89.72^\circ$. The flexural rays with the azimuth angle $89.72^\circ \leq \theta \leq 90^\circ$ which are in the close proximity to the edge of ABH indentation escape from the indentation. Total focalization of incident waves in the ABH indentation can be achieved when $m=3$. Therefore, the conventional ABH indentation with larger index m definitely exhibits better wave focalization ability.
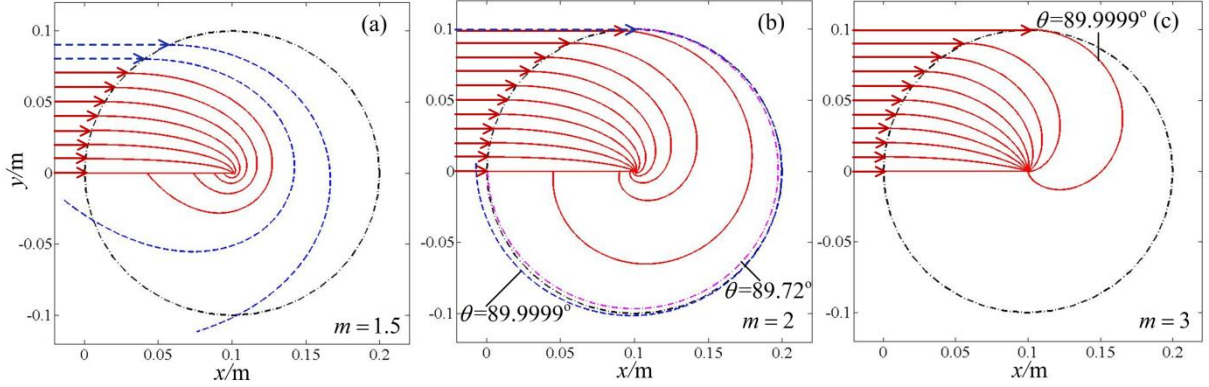
Fig. 8. The trajectories of flexural wave propagation in conventional ABH indentations with power-law profile ($h_1 = r_1 = 0$).

4.2. Flexural Ray Trajectory in generalized ABH Indentations

As mentioned before, the extra thickness is prone to exist in ABH structures in the machining process, which is observed to have the most impact on the position of energy focalization [13]. In order to demonstrate the specific propagation path of the flexural waves in generalized ABH indentations with extra thickness, the ray trajectories are calculated with results shown in Fig. 9. The influence of the extra thickness h_1 as well as the power index m on the flexural rays is investigated. The wave transmission in the generalized ABH indentations with an extra thickness $h_1 = 0.001$m and $h_1 = 0.0005$m with index $m=1.5$, $m=2$ and $m=3$ are compared. It can be observed from the results that flexural ray trajectories still deflect inward in the indentation. However, the focusing characteristic changes compared with that in the conventional ideal ABH indentations. Energy focalization can still be obtained to certain extent, as evidenced by a small area of high concentration of the bent rays. With the present symmetric wave incidence, the flexural ray trajectories converge to the symmetric line downstream the central point, but not to a single point as long as the ABH indentation contains an extra thickness. In these circumstances, the curvature of the trajectories and the focusing level of the flexural waves are greatly influenced by the refractive index, which can be enhanced with a larger m. The extra thickness mainly effects the position of energy focalization, which is closer to the center with a smaller h_1.
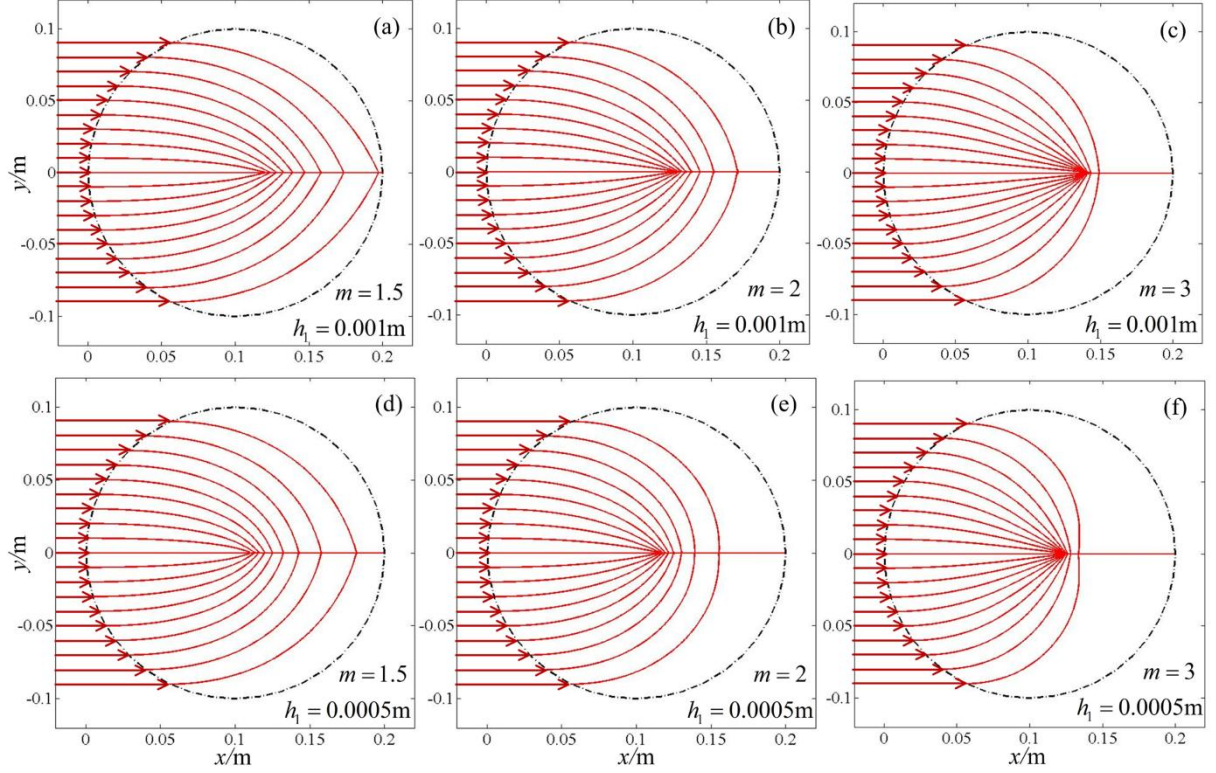
Fig. 9. The trajectories of flexural wave propagation in plates with imperfect ABH indentations ($h_1 \neq 0$, $r_1 = 0$).

Figure 10 depicts the ray trajectories of the flexural wave propagation in plates with another type of imperfect ABH indentations ($h_1 \neq 0$, $r_1 \neq 0$). The radius of the central plateau is 0.02m. It can be seen that with an extra thickness $h_1 = 0.001$m, part of the flexural waves propagate into the central plateau, while the other part detours around the central plateau. This explains the different energy focalization phenomena observed in the previous work [13], in which it was observed that the energy focuses to a confined region slightly downstream of the center plateau. The trajectories in plateau region are straight lines. As a way to enhance wave gathering in a region such as a plateau, a smaller h_1 would certainly help. In fact, with a thinner extra thickness ($h_1 = 0.0002$m), as demonstrated in Fig. 10(d)-(f), much more flexural rays pass through the plateau compared with those in Fig. 10(a)-(c). Although the curvature of the ray trajectories depends on both h_1 and m, the percentage of the captured energy, however, only depends on h_1. The flexural ray trajectories propagate into the scope of the plateau through shorter routes with a larger m. Therefore, effective wave focalization in a confined region such as a central plateau within the ABH indentation can be achieved through appropriate parameter design.
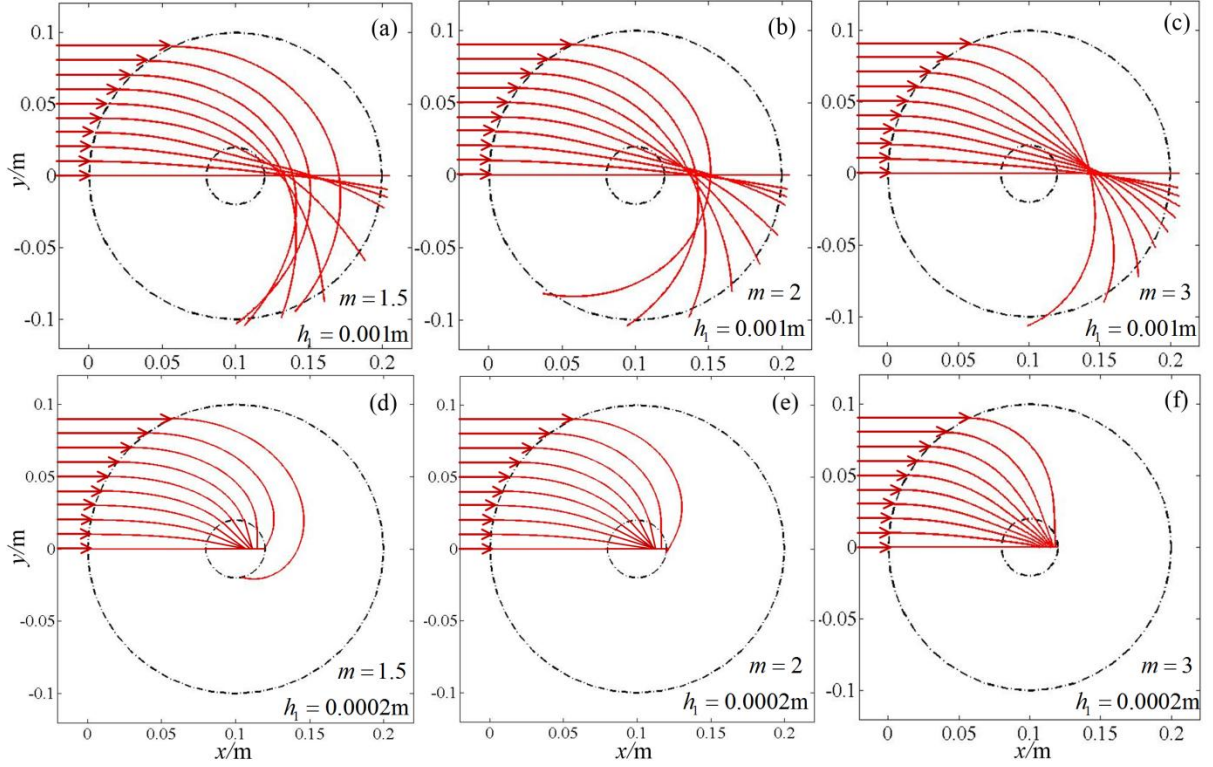
Fig. 10. The trajectories of flexural wave propagation in plates with imperfect ABH indentations ($h_1 \neq 0$, $r_1 = 0.02$m).

5. Conclusions

In this study, a numerical integration scheme of the flexural ray equation was proposed and used to predict the ray trajectories of flexural waves in generalized ABH indentations for the investigations of the wave propagation and focalization properties. The feasibility of the method was verified through comparison with experimental results and FEM simulations. The method was applied to both conventional ABHs satisfying the power law thickness profile relation and the other two types of generalized ABHs with different geometrical parameters. The following conclusions can be drawn:

1). The conventional ABH indentation with a larger power index m exhibits better effect of wave focalization. There exists a critical trajectory in the ideal ABH indentation which separates the rays that converge to the center and those that diverge. The ratio of the rays converging to the center is 99.69% in the ideal ABH case investigated in this paper. When $m = 3$ or above, total wave focalization can be achieved.

2). The rays bend towards the symmetry axis of the ABH, but do not converge to a single point in the ABH indentations with an extra plate thickness. Partial energy focalization can still be obtained, evidenced by the existence of a confined area containing high concentration of bent rays. The power index m and the extra thickness h_1 affect the curvature of the ray trajectory, as well as the position and the intensity of the energy

focalization. The wave focalization can be enhanced with a larger m and a smaller h_1.

3). In the generalized ABH indentations with a central plateau, only a portion of the rays can enter the indentation and captured by the plateau. Although the curvature of the ray trajectories depend on both the extra thickness h_1 and the power index m, the percentage of the captured energy, however, only depends on the extra thickness , not the power index.

As a final remark, effective and tunable wave focalization within a confined region within the generalized ABH indentations is possible. For a given application, the ABH configuration being considered in this work is general and provides several geometrical parameters to be eventually tuned for achieving the optimized ABH performance without compromising the structural integrity. To this end, the proposed analysis tool becomes important, and it provides guidance for the arrangement of the damping layer. Because of the main focus of this paper, damping layers were not considered. With visco-elastic damping layers arranged strategically over the energy focalization area, based on the prediction of the ray trajectories, the damping characteristics as well as the efficiency of the energy dissipation of the ABH structures need to be systematically investigated in the next stage of research. Moreover, the proposed analysis method can also be extended to analyze flexural ray properties in other ABH structures or even inhomogeneous structures with continuous variation of the refractive index.

References

[1] V.V. Krylov, New type of vibration dampers utilising the effect of acoustic'black holes', Acta Acustica united with Acustica, 90 (2004) 830-837.

[2] V.B. Georgiev, J. Cuenca, F. Gautier, L. Simon, V.V. Krylov, Damping of structural vibrations in beams and elliptical plates using the acoustic black hole effect, Journal of Sound and Vibration, 330 (2011) 2497-2508.

[3] L. Zhao, S.C. Conlon, F. Semperlotti, Broadband energy harvesting using acoustic black hole structural tailoring, Smart Materials and Structures, 23 (2014) 065021.

[4] V.V. Krylov, F.J.B.S. Tilman, Acoustic 'black holes' for flexural waves as effective vibration dampers, Journal of Sound and Vibration, 274 (2004) 605-619.

[5] V.V. Krylov, Propagation of plate bending waves in the vicinity of one- and two-dimensional acoustic black hole, Proceedings of the ECCOMAS International Conference on Computational Methods in Structural Dynamics and Earthquake Engineering (COMPDYN 2007), Rethymno, Crete, Greece, 2007, pp. CD-ROM.

[6] D.J. O'Boy, V.V. Krylov, Damping of flexural vibrations in circular plates with tapered central holes, Journal of

Sound and Vibration, 330 (2011) 2220-2236.

[7] E.P. Bowyer, D.J. O'Boy, V.V. Krylov, F. Gautier, Experimental investigation of damping flexural vibrations in plates containing tapered indentations of power-law profile, Applied Acoustics, 74 (2013) 553-560.

[8] E.P. Bowyer, V.V. Krylov, Experimental investigation of damping flexural vibrations in glass fibre composite plates containing one- and two-dimensional acoustic black holes, Composite Structures, 107 (2014) 406-415.

[9] L. Zhao, S. Conlon, F. Semperlotti, Experimental verification of energy harvesting performance in plate-like structures with embedded acoustic black holes, INTER-NOISE and NOISE-CON Congress and Conference Proceedings, Institute of Noise Control Engineering, 2015, pp. 4043-4050.

[10] H.F Zhu, F. Semperlotti, Phononic thin plates with embedded acoustic black holes, Physical Review B, 91 (2014) 39-43.

[11] V.V. Krylov, Acoustic black holes: Recent developments in the theory and applications, IEEE transactions on ultrasonics, ferroelectrics, and frequency control, 61 (2014) 1296-1306.

[12] A. Climente, D. Torrent, J. Sánchez-Dehesa, Gradient index lenses for flexural waves based on thickness variations, Applied Physics Letters, 105 (2014) 064101.

[13] W. Huang, H.L Ji, J.H Qiu, L. Cheng, Wave energy focalization in a plate with imperfect two-dimensional acoustic black hole indentation, Journal of Vibration and Acoustics, 138 (2016) 061004.

[14] V.V. Krylov, Transmission of a Rayleigh wave across smooth large-scale surface irregularities, Soviet Physics – Acoustics, 34 (1988) 613-618.

[15] V.V. Krylov, Conditions for validity of the geometrical-acoustics approximation in application to waves in an acute-angle solid wedge, Soviet Physics – Acoustics, 35 (1989) 176-180.

[16] A.M. Lomonosov, S.L. Yan, B. Han, H.C. Zhang, Z.H. Shen, Orbital-type trapping of elastic Lamb waves, Ultrasonics, 64 (2016) 58-61.

[17] S.L. Yan, A.M. Lomonosov, Z.H. Shen, Numerical and experimental study of Lamb wave propagation in a two-dimensional acoustic black hole, Journal of Applied Physics, 119 (2016) 214902.

[18] L.L Tang, L. Cheng, Enhanced Acoustic Black Hole effect in beams with a modified thickness profile and extended platform, Journal of Sound and Vibration, 391 (2016) 116-126.

[19] A. W. Leissa, Vibration of Plates, Scientific and Technical Information Division, NASA, (1969).

[20] P.A. Feurtado, S.C. Conlon, An Experimental Investigation of Acoustic Black Hole Dynamics at Low, Mid, and High Frequencies, Journal of Vibration and Acoustics, 138 (2016) 061002.

[21] L.L Tang, L. Cheng, Broadband locally resonant band gaps in periodic beam structures with embedded acoustic black holes, Journal of Applied Physics, 121 (2017) 605.

[22] A. Climente, D. Torrent, J. Sánchez-Dehesa, Omnidirectional broadband acoustic absorber based on metamaterials, Applied Physics Letters, 100 (2012) 144103.

[23] C. Zhang, J.H. Qiu, H.L. Ji, Laser ultrasonic imaging for impact damage visualization in composite structure, EWSHM - 7th European workshop on structural health monitoring, 2014, pp. 2199-2205.

[24] Y.C Wu, J.H. Qiu, C Zhang, K.J. Zhu, H.L. Ji, A method to improve the visibility of the damage-reflected wave, Chinese Journal of Lasers, 41 (2014) 0308001-20.

[25] C. Zhang, H.L. Ji, J.H. Qiu, Y.C. Wu, Research on Interference Energy Calculation Method in Laser Ultrasonic Technique, Acta Optica Sinica, 34 (2014) 714001-30.

[26] W.H. Prosser, M.R. Gorman, J. Dorighi, Extensional and Flexural Waves in a Thin-Walled Graphite/Epoxy Tube, Journal of Composite Materials, 26 (1992) 418-427.

[27] A.N. Norris, V.V. Krylov, I.D. Abrahams, Flexural edge waves and comments on "A new bending wave solution for the classical plate equation", Journal of the Acoustical Society of America, 107 (2000) 1781-1785.

[28] H.P. Lee, S.P. Lim, M.S. Khun, Diversion of energy flow near crack tips of a vibrating plate using the structural intensity technique, Journal of Sound and Vibration, 296 (2006) 602-622.

[29] N.K. Mandal, R.A. Rahman, M.S. Leong, Experimental investigation of vibration power flow in thin technical orthotropic plates by the method of vibration intensity, Journal of Sound and Vibration, 285 (2005) 669-695.

[30] J.H. Zhang, B. Han, Analysis of engine front noise using sound intensity techniques, Mechanical Systems and Signal Processing, 19 (2005) 213-221.
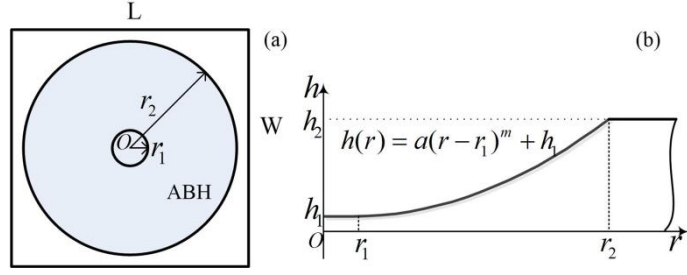
L

W

(a)

(b)

r_2

r_1

ABH

h

h_2

h_1

$h(r) = a(r - r_1)^m + h_1$

O

r_1

r_2

r

Fig. 1. Plate with a generalized two-dimensional acoustic black hole indentation.

$\alpha = 0$

ds

$\mathbf{r}(s)$

$\mathbf{r} + d\mathbf{r}$

θ

O

ABH

r

Fig. 2. Sketch of incident wave and wave trajectory.

AE sensor

Signal conditioner

PC

Start point

Laser mirror scanner

Q-switch laser generator

(a)

AE sensor M31

Plate with indentation

Q-switch laser generator

Signal conditioner

Laser mirror scanner

Data acquisition system with PC

(b)
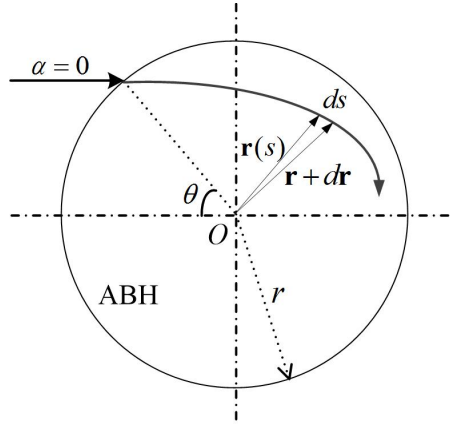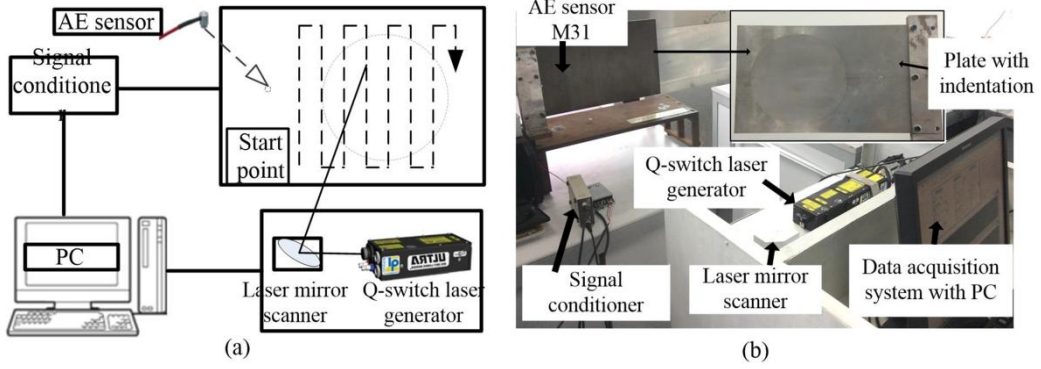
Fig. 3. Schematic diagram (a) and experiment setup (b) of the laser ultrasonic system.
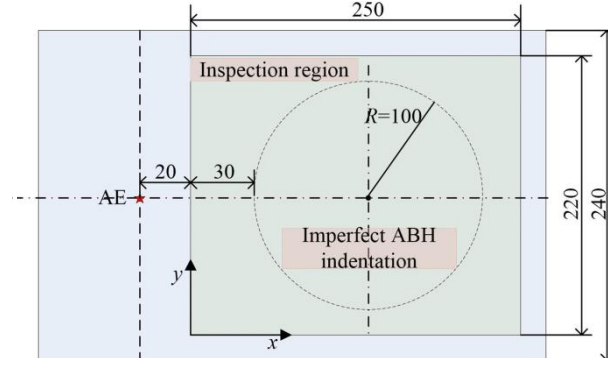
Fig. 4. Diagrammatic sketch of experimental plate.
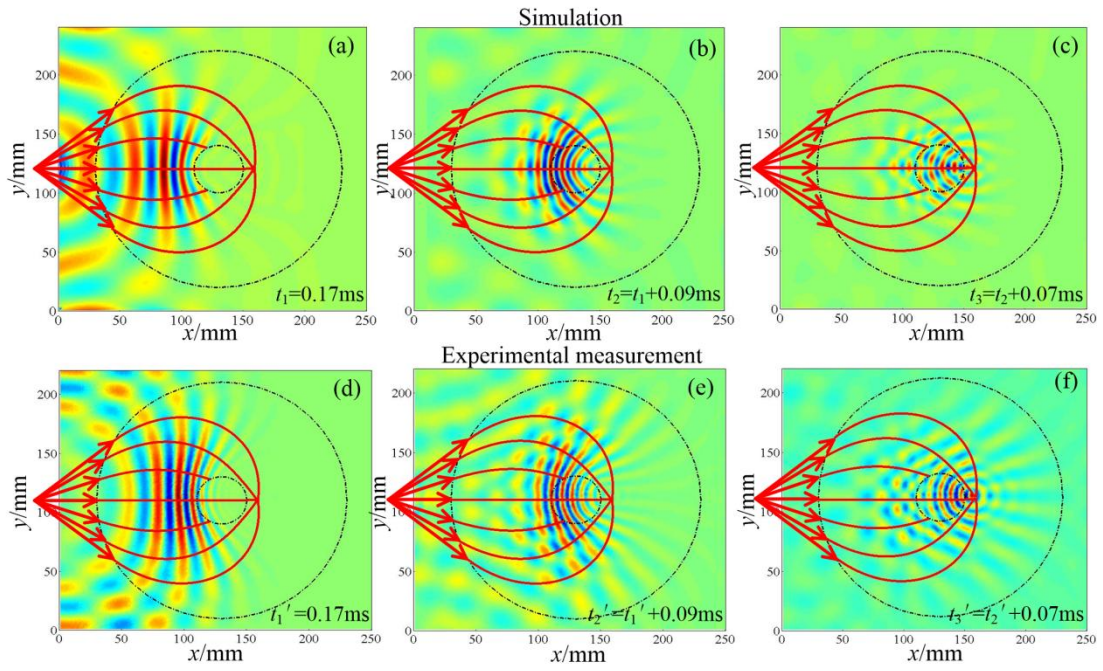
Fig. 5. Comparison between the simulated wave fields with the ray paths ((a)-(c)) and the measured ones ((d)-(f)). The curves with arrows represent the ray trajectories ($m=2$, $r_1=0.02$m, $h_1=0.0006$m).
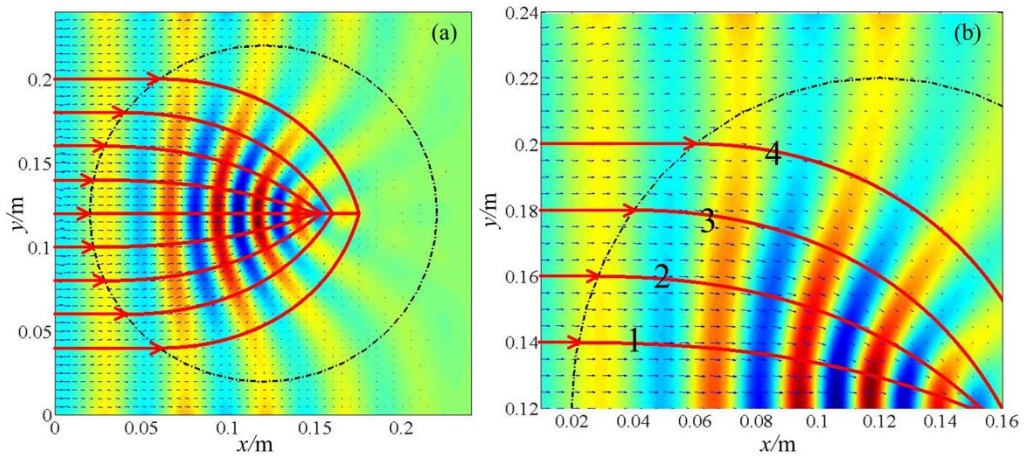
Fig. 6. Comparison of power flow vectors (FEM) with the ray paths (GA) in the ABH indentation with $m = 2$, $h_1 = 0.001\text{m}$.
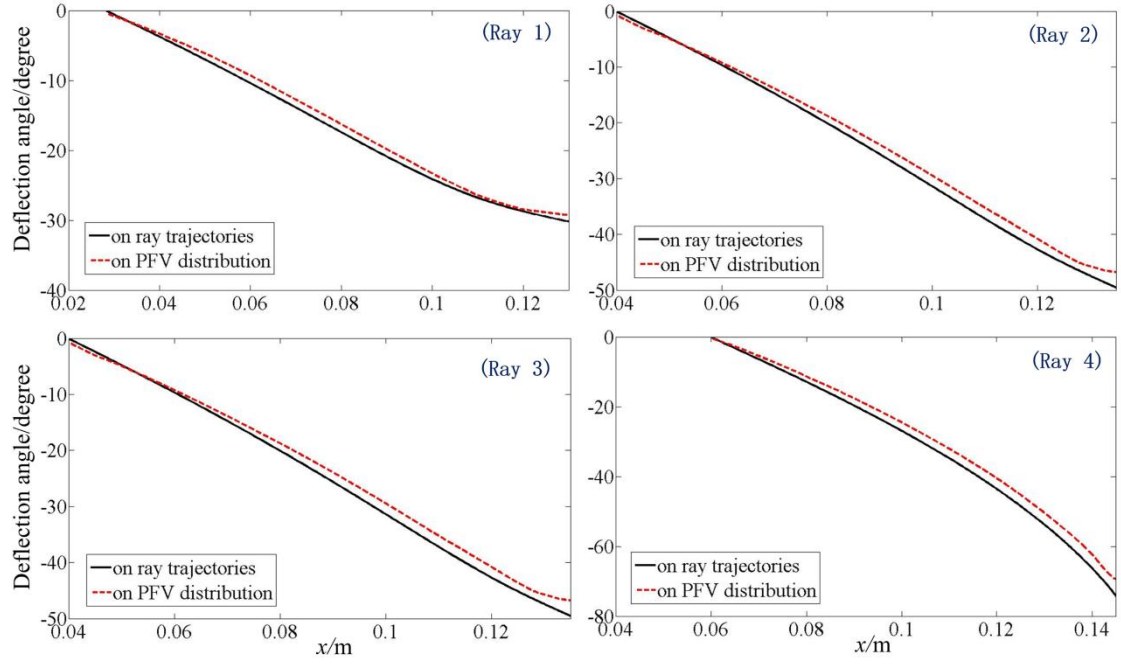

Fig. 7. Comparison of deflection angle on four ray trajectories with the deflection angle of power flow vectors on the corresponding position.
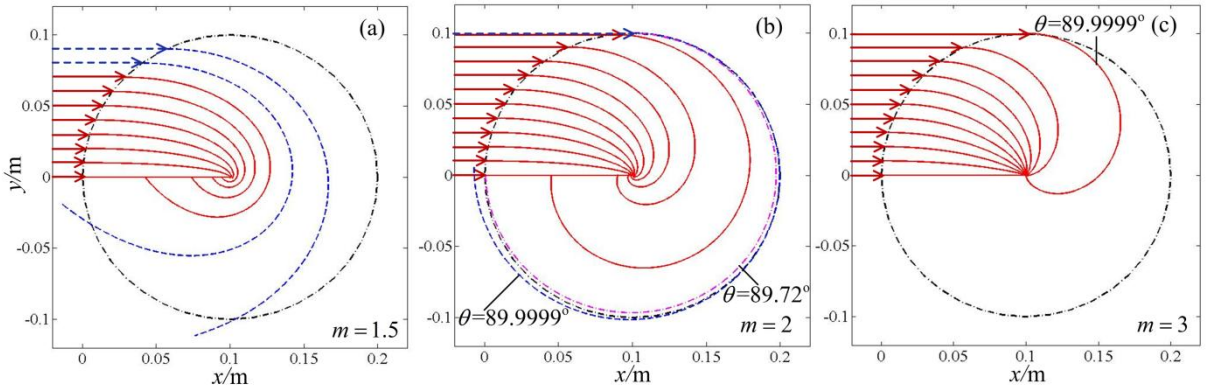

Fig. 8. The trajectories of flexural wave propagation in conventional ABH indentations with power-law profile ($h_1 = r_1 = 0$).
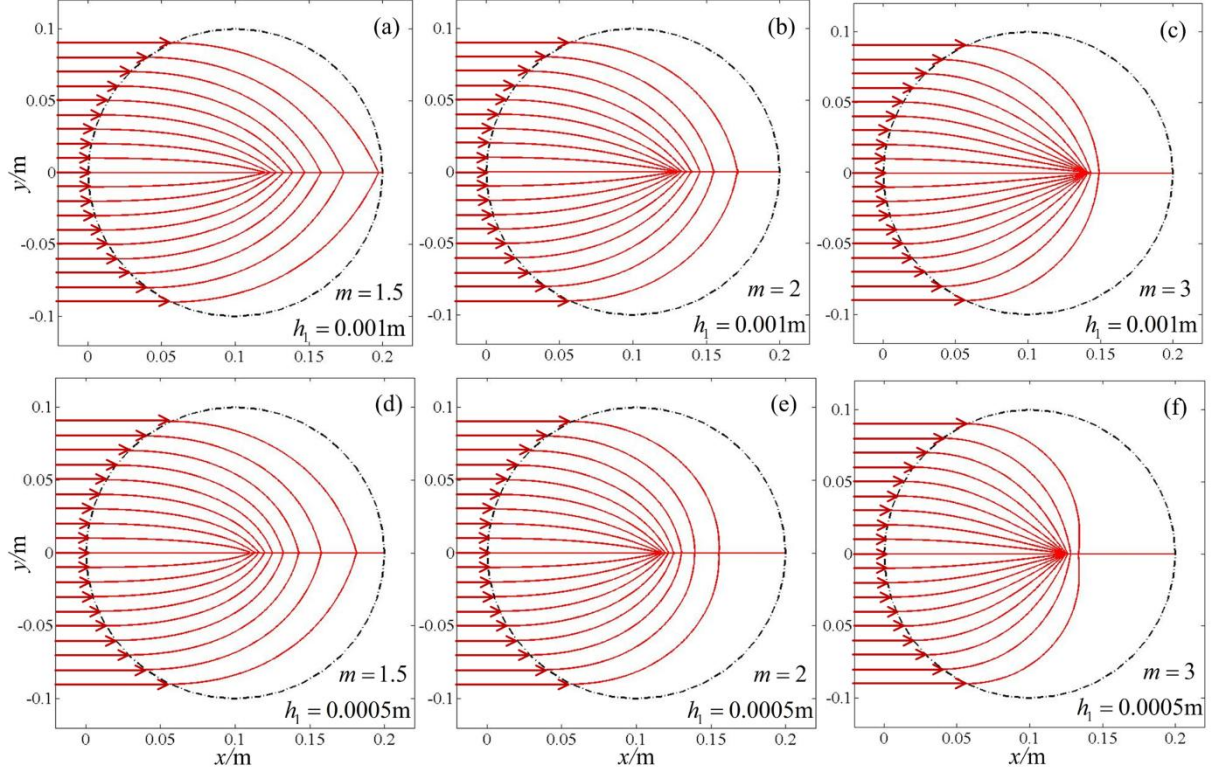
Fig. 9. The trajectories of flexural wave propagation in plates with imperfect ABH indentations ($h_1 \neq 0$, $r_1 = 0$).
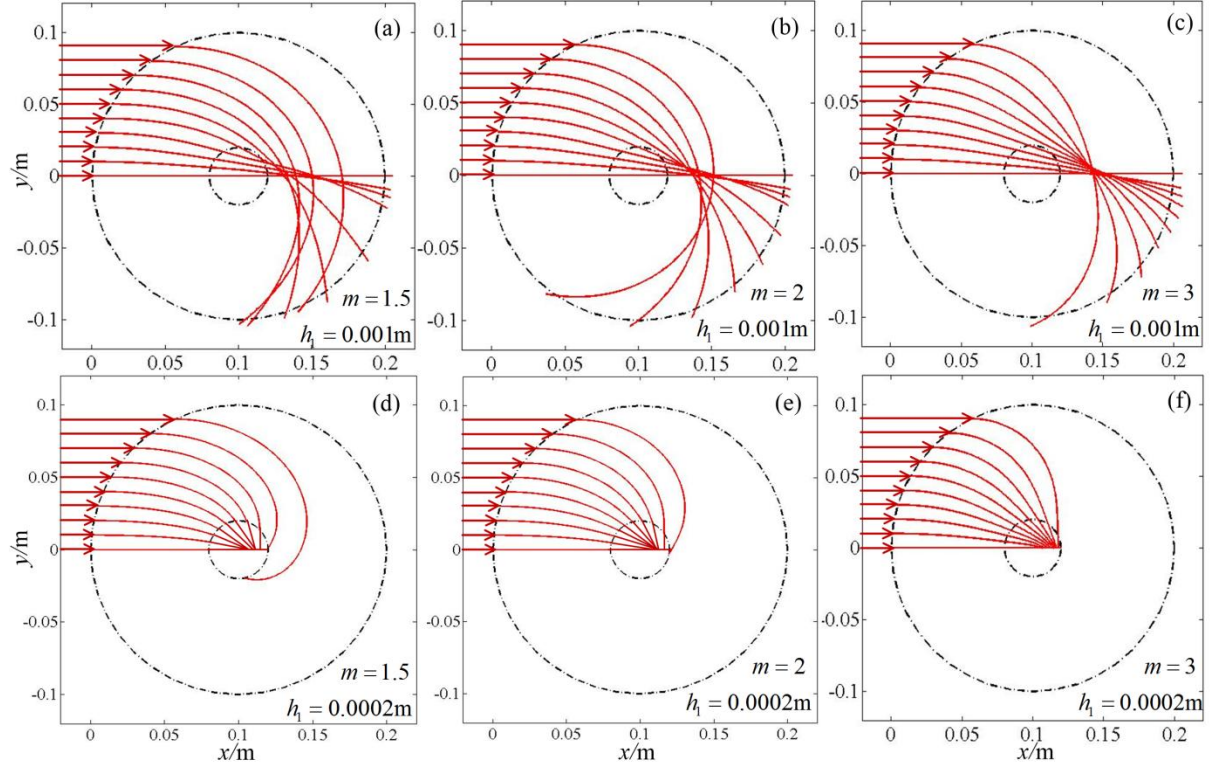

Fig. 10. The trajectories of flexural wave propagation in plates with imperfect ABH indentations ($h_1 \neq 0$, $r_1 = 0.02$m).